

Energy reconstruction at high energy with the LAT

Ph. Bruel
LLR, Ecole Polytechnique,
91128 Palaiseau, France

October 17, 2005

1 Introduction

The task of the LAT is to detect gamma rays and measure their incoming direction and energy throughout a very large phase space : from 30 MeV to 300 GeV with a field of view more than 2.5 sr wide. Because of the LAT geometry (the tracker is $\sim 1.4 X_0$ thick and the calorimeter is $\sim 8.6 X_0$ thick for normally incident gammas), the fraction of energy deposited in the tracker and in the calorimeter vary much through this large phase space. Figure 1(left) shows the mean of the fraction of the energy deposited in the calorimeter as function of the logarithm of the energy for tracker events almost on-axis. This fraction is maximum at ~ 1 GeV. Below ~ 1 GeV, the energy deposited in the tracker cannot be neglected. Above ~ 1 GeV the main effect is the leakage behind the calorimeter. Another cause of energy loss is the cracks between the towers as shown in figure 1(right). The large variety of configurations makes the energy reconstruction a non trivial task and a method based on only one piece of information (i.e. the energy deposited in the calorimeter) is unlikely to work optimally for all of them.

This note presents a method, called `CalFullProfile` according to the name of the implemented algorithm, that reconstructs the energy of rather high energy gamma rays (above ~ 1 GeV), i.e. when the energy deposited in the tracker tends to be small compared to the energy deposited in the calorimeter and when the leakage behind the calorimeter can be large.

2 Basic principles

The longitudinal segmentation of the calorimeter ($\sim 1.1 X_0$ per layer) provides information about the shower shape. The longitudinal profile of the energy deposition of electromagnetic showers is well known. As a consequence, in order to determine the energy of an incoming gamma ray, a way to take advantage of the calorimeter longitudinal segmentation is to find the profile which fits the best with the layer energies. Such a fit is also a good way to overcome the leakage problem.

A profile fitting algorithm for the LAT has already been implemented [1]. It is based on the knowledge of the average longitudinal profile whose parameters depend on energy. The average profile is very useful when the available information is scarce, i.e. when the shower is poorly contained. But showers fluctuate, so using an average profile when the shower is relatively well (but not completely) contained is unlikely to give the best resolution. A natural way to try to improve the resolution is then to take into account the shower fluctuations. This implies to parameterize the profile parameters and their fluctuations as function of energy. Then, during the fit, one should constrain the parameters depending on the containment of the shower : the less the shower is contained, the more the profile should tend towards the average profile.

For a given shower profile, the computation of the energy deposited in the layers requires to translate the trajectory of the gamma ray in radiation length units. This requires knowing the amount of active and inactive material in the LAT seen by the gamma ray which is very sensitive to its trajectory. For quasi on-axis gamma rays entering the calorimeter at the center of a tower, the longitudinal development of the shower is the only piece of information needed because of the layer structure of the calorimeter and because the shower is far away from cracks. But knowledge of the radial profile becomes essential as soon as the shower is close to the towers boundaries, or when its axis is not perpendicular to the layer planes anymore.

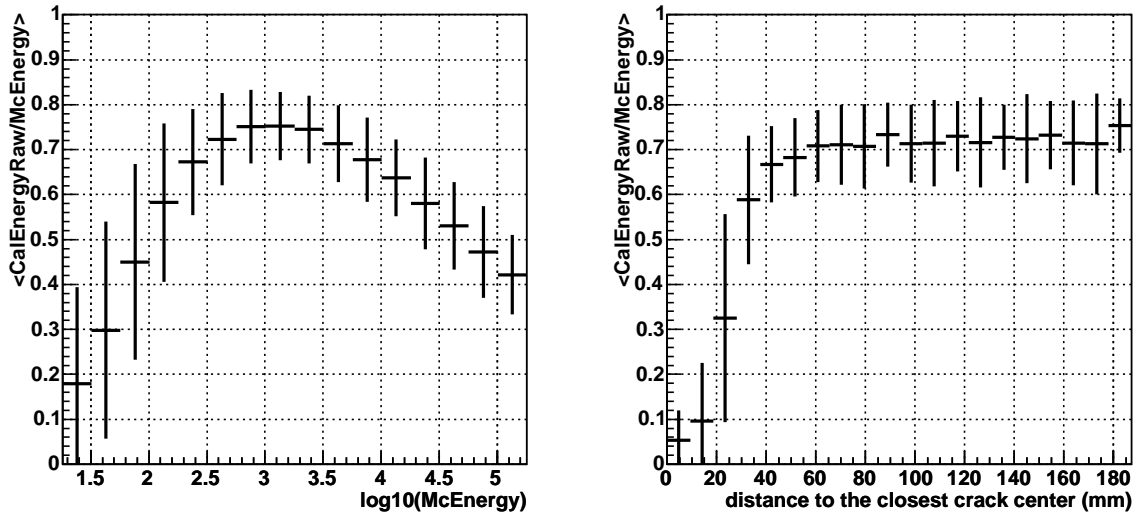


Figure 1: Left : the mean (and rms) of the fraction of the energy deposited in the calorimeter as function of the logarithm of the energy for tracker events almost on axis ($McZDir < -0.99$) and whose impact point is less than 10 cm away from the center of a tower. Right : the mean (and rms) of the fraction of the energy deposited in the calorimeter as function of the distance of the impact point to the closest crack center for tracker events almost on axis ($McZDir < -0.99$) and whose energy is between 1 and 10 GeV.

In brief, the basic principles of `CalFullProfile` are :

- a computation of the trajectory of the gamma ray inside the LAT in units of radiation length using a tridimensional model of electromagnetic showers;
- a parameterization of the profile parameters and their fluctuations as function of energy;
- the parameters describing the profile are more or less constrained during the fit, depending on the shower containment.

3 Profile parameterization

The spatial energy distribution of electromagnetic showers can be described by a longitudinal profile and a radial profile. Since the radial profile depends on the position in the shower, the longitudinal will be discussed first.

3.1 Longitudinal parameterization

The average longitudinal shower profile can be described by a gamma distribution [2]:

$$\left\langle \frac{dE(t)}{dt} \right\rangle = E \times \frac{(\beta t)^{\alpha-1} \beta e^{-\beta t}}{\Gamma(\alpha)}$$

where t is the longitudinal shower depth in units of radiation length, α the shape parameter and β the scaling parameter. The center of gravity $\langle t \rangle$ and the depth of the maximum T depend on α and β according to :

$$\langle t \rangle = \frac{\alpha}{\beta} \quad T = \frac{\alpha - 1}{\beta}$$

The same function can also be used to describe individual profiles. Following the approach of [3], the two chosen parameters besides E are α and the shower maximum T , leading to the following function for the longitudinal profile :

$$\frac{dE(t)}{dt} = E \times \frac{(\alpha - 1)}{T\Gamma(\alpha)} ((\alpha - 1)t/T)^{\alpha-1} e^{-(\alpha-1)t/T} \quad (1)$$

The choice of T is motivated by its impact on the description of the shower profile, in particular the radial profile, and on the estimation of the containment.

In order to study the dependence of the profile parameters with energy, simulations of gamma rays in an infinite CsI calorimeter were performed with `Geant4` at various energies (ranging from 5 to 150 GeV). The calorimeter was segmented in 1.85 mm ($0.1 X_0$) slices. For each event, the conversion point is used to define the shower starting point $t = 0 X_0$. In order to smooth the longitudinal profile and to come closer to the LAT calorimeter geometry (the height of a log is $19.9/18.5 \sim 1.1X_0$), $1 X_0$ bins were used to construct the histogram of the longitudinal profile. This histogram is fitted using `minuit`. It was empirically found that applying an error $= 0.02\sqrt{E/1 \text{ GeV}}$ to each bin leads to $\langle \chi^2/\text{ndf} \rangle \sim 1$. Figure 2 shows examples of individual profiles of 10 GeV gammas.

Figures 3 and 4 show the distributions of the fit parameters for 10 GeV and 100 GeV gammas. The distributions of α and T can be fitted with a lognormal. In order to deal with distributions as gaussian as possible, $\ln \alpha$ and $\ln T$ are used rather than α and T . The distribution of $\ln T$ is not as gaussian as the distribution of $\ln \alpha$ but the maximum and the sigma given by the lognormal fit are used as the mean and the sigma of a gaussian.

Besides the mean and sigma of $\ln \alpha$ and $\ln T$ and their correlation coefficient ρ , one has to quantify the fit error. In order to determine the residuals of the fit only showers with α and T within 30% of $\bar{\alpha}$ and \bar{T} are considered. Figure 5 shows the average profile and the residuals for 10 GeV and 100 GeV gammas. The relative error (rms of the residuals divided by the average deposited energy) is also shown and is minimal around the shower maximum. The average of this relative error around the shower maximum is used to define the relative error ϵ which will be used in the profile fit as a modelization error.

Figure 6 shows how all the parameters vary with energy. The parameterizations given by [3] are used :

$$\begin{aligned} \overline{\ln \alpha}(E) &= \ln(p_0 + p_1 \ln E) \\ \sigma_{\ln \alpha}(E) &= (p_0 + p_1 \ln E)^{-1} \\ \overline{\ln T}(E) &= \ln(p_0 + \ln E) \\ \sigma_{\ln T}(E) &= (p_0 + p_1 \ln E)^{-1} \\ \rho(E) &= p_0 - p_1 e^{-E/p_2} \\ \epsilon(E) &= p_0 E^{p_1} \\ \text{bias}(E) &= \min(\ln(p_0 + p_1 \ln E), 0.99) \end{aligned}$$

Because the profile fit underestimates slightly the energy (-2 to -1%), the bias is parameterized and the energy given by the fit is corrected for this bias.

3.2 Radial parameterization

Following [3] we use the following two components function for the normalized average radial profile (which is assumed to be uniform in ϕ) :

$$rf(\tau, r) = \frac{1}{dE(t)} \frac{dE(t, r)}{dr} = p(\tau) \frac{2R_C^2(\tau)}{(r^2 + R_C^2(\tau))^2} + (1-p(\tau)) \frac{2R_T^2(\tau)}{(r^2 + R_T^2(\tau))^2} \quad \left(\Rightarrow \int_0^\infty rf(\tau, r) dr = 1 \right)$$

where $R_C(\tau)$ ($R_T(\tau)$) is the median of the core (tail) component and $p(\tau)$ gives the relative weight of the core component ($0 \leq p\tau \leq 1$). This average radial profile depends on the longitudinal position in the shower, i.e. on $\tau = t/T$. In order to determine how R_C , R_T and p vary with τ , a simulation was performed with `Geant4`. In this case the CsI calorimeter was divided longitudinally in $X_0/4$ slices and radially in $R_M/4$ slices (The Moliere radius, R_M , is 3.5 cm for CsI). For each event, the shower maximum is determined as described in the previous section. The integrated average radial profile is computed for

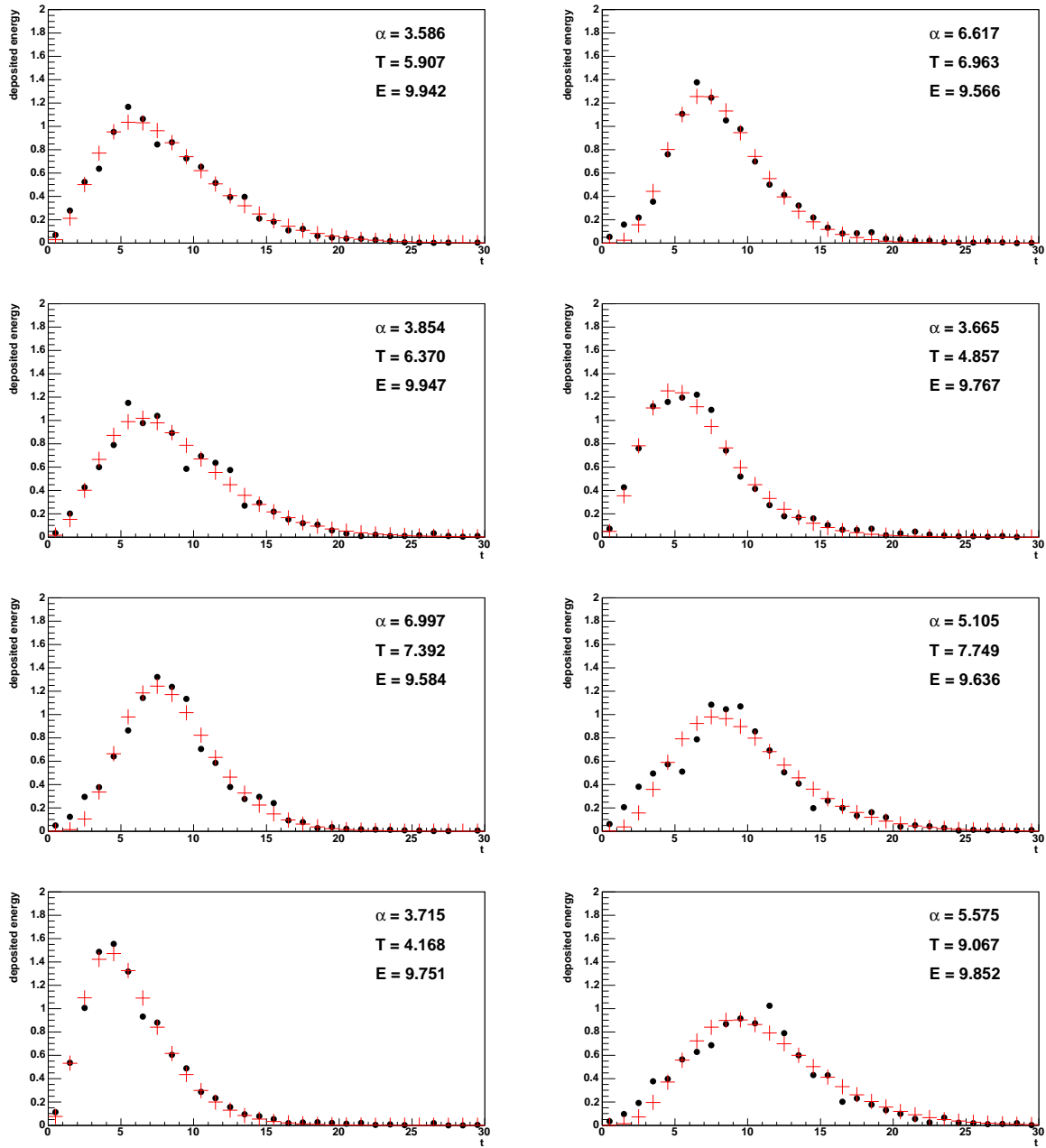


Figure 2: Individual profiles of 10 GeV gammas : deposited energy (\bullet) and the result of the fit ($+$). It is interesting to note that for tracker events on axis in GLAST, the end of the calorimeter, in these histograms, lies between 8.6 and $8.6 + 1.4 = 10 X_0$, depending on the position of the vertex.

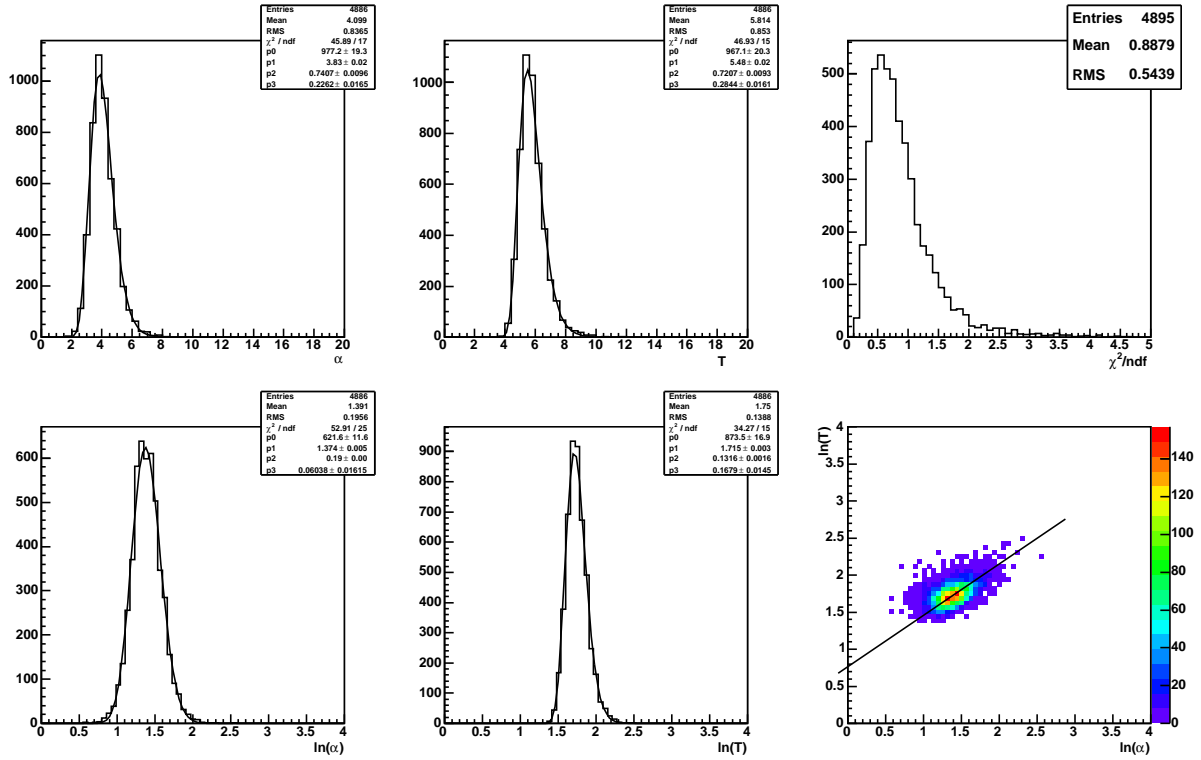


Figure 3: Fit parameters distribution for 10 GeV gammas.

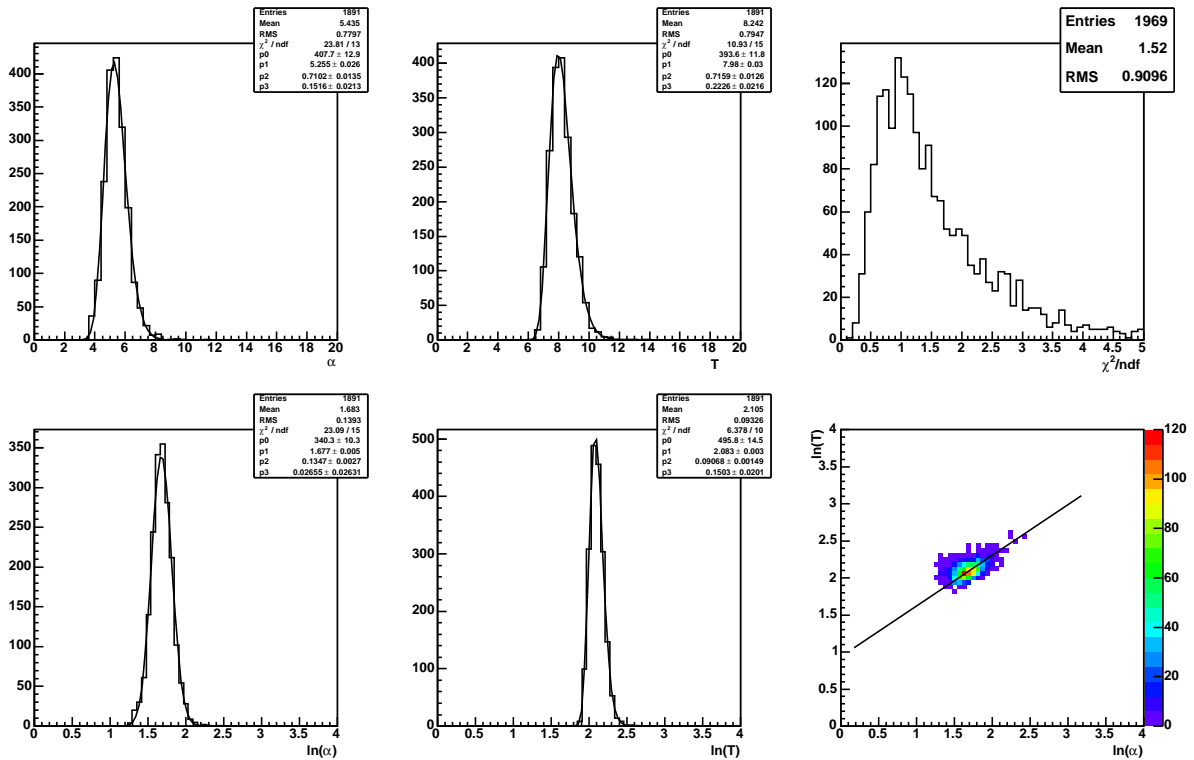


Figure 4: Fit parameters distribution for 100 GeV gammas.

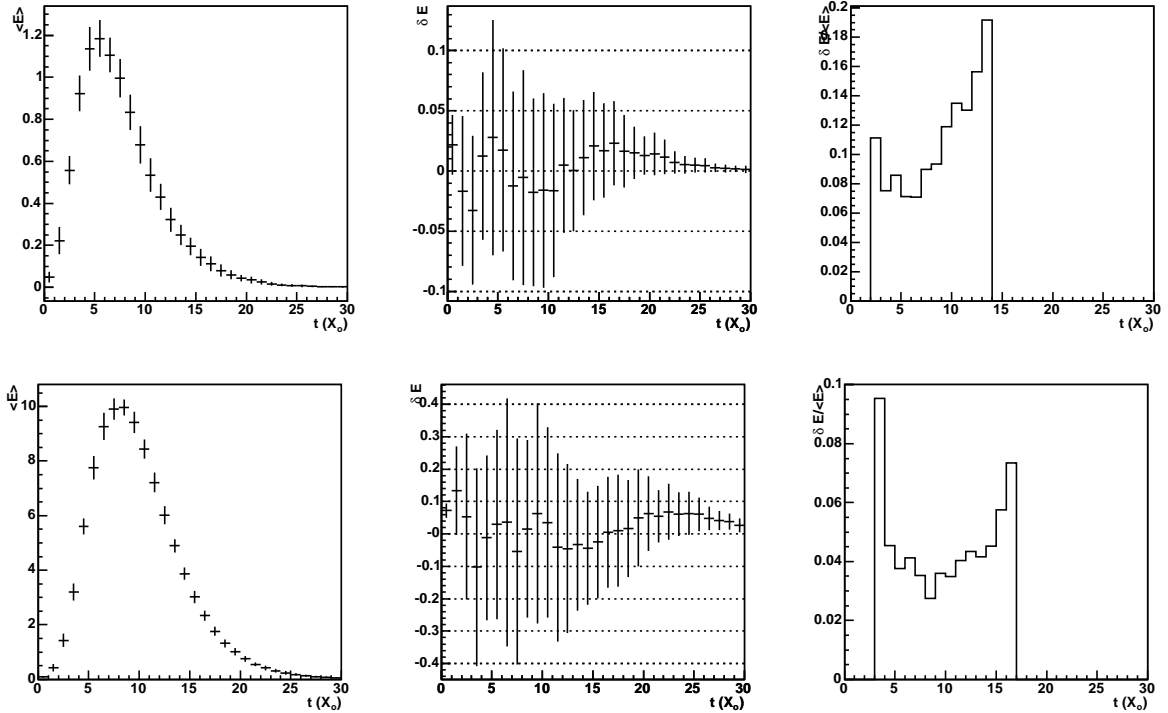


Figure 5: Fit error study for 10 GeV (up) and 100 GeV (bottom) gammas. Left : profile as a function of longitudinal shower depth t (mean and rms). Center : residuals as function of t (mean and rms). Right : relative error as function of t .

various intervals of the position in the shower. Figure 7 shows these profiles for 10 GeV gammas. The fit of each profile allows the determination of R_C , R_T and p for various intervals of the position in the shower.

The functions used for the fits are as in [3]:

$$\begin{aligned}
 R_C(\tau) &= p_0 + p_1\tau \\
 R_T(\tau) &= p_0(e^{p_2(\tau-p_1)} + e^{p_3(\tau-p_1)}) \\
 p(\tau) &= p_0e^{(p_1-\tau)/p_2 - e^{(p_1-\tau)/p_2}}
 \end{aligned}$$

Figure 8 shows how these parameters vary with τ . Since there is no obvious energy dependence the results at 10 GeV are used to define the radial profile of gamma showers. One can use these R_C , R_T and p parameterizations to compute effective radii, that is to say the radii containing a given fraction of energy. Figure 9 shows the 68, 80 and 90% effective radii. The behaviour of R_T at small τ is mainly due to the propagation of low energy photons that do not really contribute to the development of the shower. In order to neglect this effect and because R_T is overestimated by the fit for $\tau < 0.25$, the radial profile for $\tau < 0.25$ is chosen to be fixed to its shape at $\tau = 0.25$.

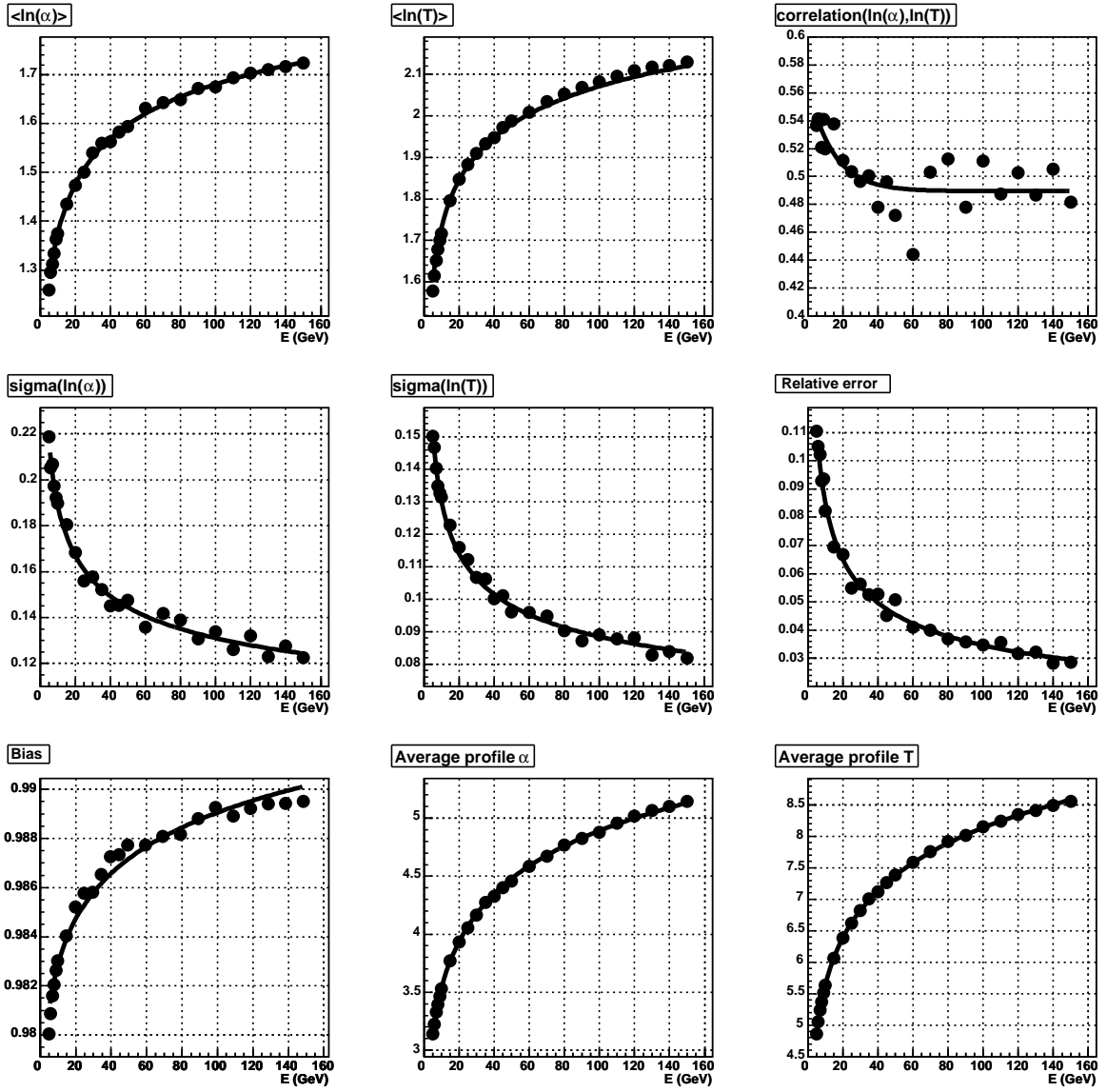


Figure 6: Energy parameterization of the profile parameters.

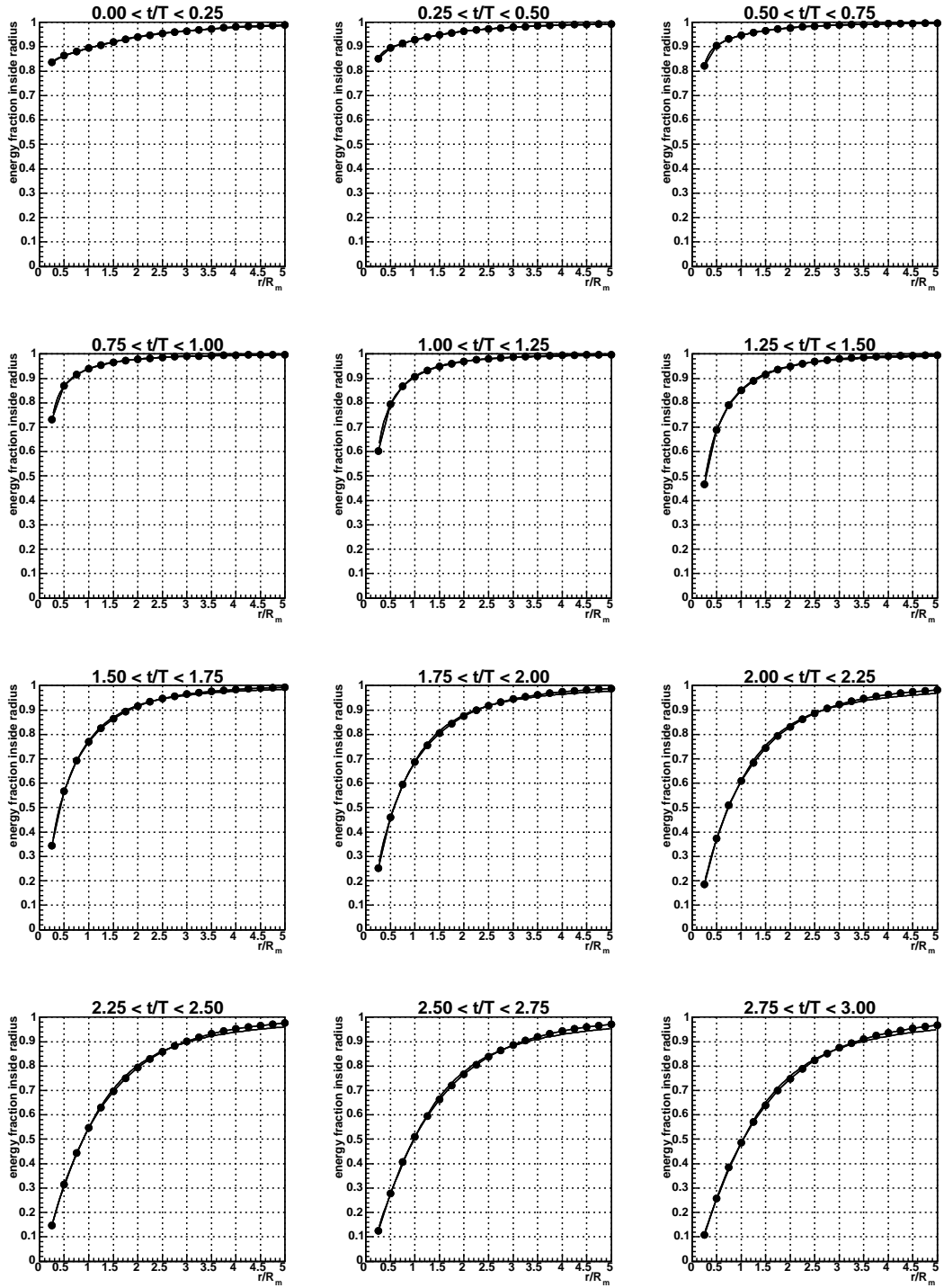


Figure 7: Integrated radial profiles ($\int_0^T \rho f(\tau, \rho) d\rho$) for various positions in the shower for 10 GeV gammas.

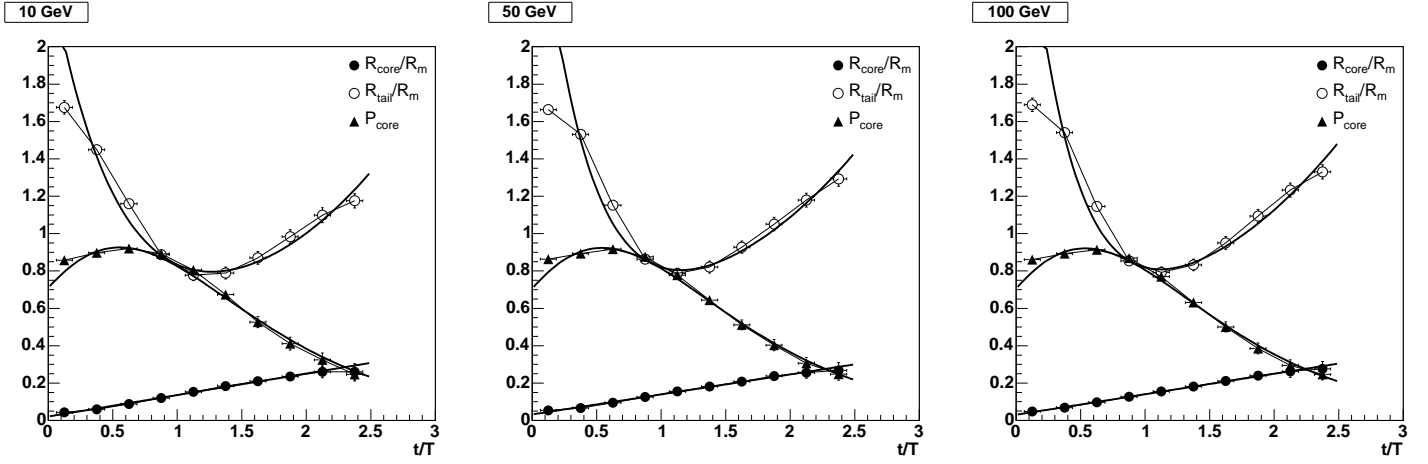


Figure 8: The three parameters describing the radial profile, $R_C(\tau)$, $R_T(\tau)$ and $p(\tau)$, for 10 (left), 50 (center) and 100 GeV (right) gammas.

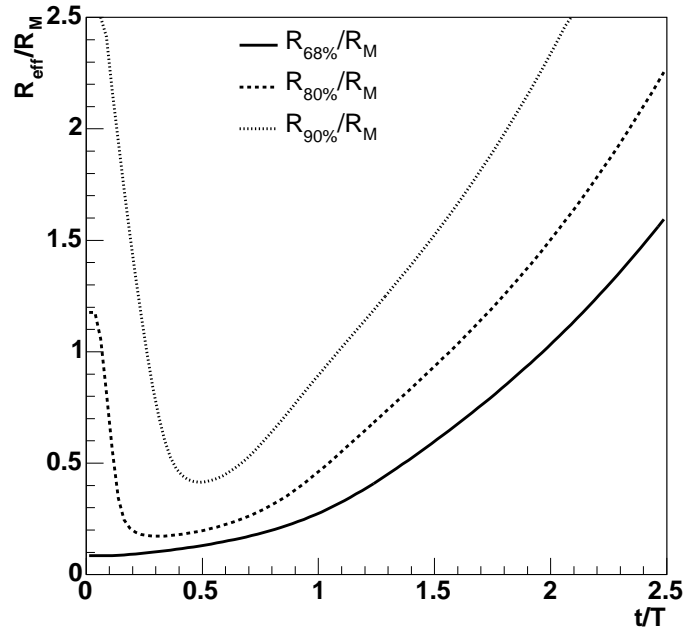


Figure 9: Effective radius for 68, 80, 90% containment as function of t/T .

4 Development of showers in the calorimeter

Since the shower profile is known as a function of t , the trajectory of a gamma ray through the LAT calorimeter must be translated into units of radiation length before the deposited energy in each layer can be computed. Since the radial profile is parameterized as function of the shower maximum T , this translation needs T as an input. For a given T , the description of the development of the shower in the calorimeter is done as follows :

- retrieve the trajectory information depending on the event :
 - tracker event : the starting point (i.e. corresponding to 0 X_o) is given by the tracker vertex and the direction given by the vertex direction. The entry point of the gamma ray into the calorimeter is found and the amount of radiation lengths between the starting point and the entry point is computed (considering the shower as a straight line);
 - calorimeter-only event : the starting point is the entry point of the gamma ray into the calorimeter.
- divide the trajectory into 1.85 mm steps and start 5 cm ahead of the entry point of the gamma ray into the calorimeter;
- for each step :
 - define a disk centered on the center of the step, perpendicular to the trajectory and with radius 1.5 times the 80% containment radius (which depends on t/T);
 - use 100 test points on this circle to determine the average of the following quantities (using the radial energy density as the weight) :
 - * the fraction of the shower in the “void” (i.e. outside the calorimeter volume or in the carbon cell array), inside the CsI and inside the cracks;
 - * the fraction of the energy deposited in each layer.
 - compute the amount of radiation length corresponding to the step (taking into account the active (CsI) and passive (cracks) material seen by the shower) and add it to t .
- translate all the results in functions of t , especially the fraction of the energy deposited in each layer $f_i(T, x \text{ in mm}) \rightarrow f_i(T, t \text{ in } X_0)$.

Figure 10 shows the development of one on-axis gamma shower into the LAT calorimeter. This development is easy to understand since the layers orientation makes the on-axis situation quite simple. The crenel shape of the fraction curves and the systematic difference between X and Y layers fractions results from taking into account the distance between CsI logs.

Figure 11 is more complex because the incoming angle of the gamma is now 50° . Two features can be seen : the passage through a crack (the green curve in the top figure reaches 1 and as the result the energy fraction corresponding to the second layer (in red) is ~ 0) and the energy mixing between layers (i.e. because of the radial width of the shower the energy deposited at a position t is not deposited in only one layer but shared among several layers) which increases as the shower widens.

5 Constraining the longitudinal fluctuations during the fit

For a given profile, the energy deposited in layer i is :

$$E_{prof}^i(\alpha, T, E) = \int_0^{t_{tot}} f_i(T, t) \frac{dE(t)}{dt}(\alpha, T, E) dt$$

where $\frac{dE(t)}{dt}(\alpha, T, E)$ is the longitudinal energy profile given by equation (1), $f_i(T, t)$ is the fraction of energy deposited in layer i and t_{tot} is the total amount of radiation lengths seen by the shower.

The “standard” χ^2 to be minimized for the energy reconstruction is :

$$\chi_{std}^2(\alpha, T, E) = \sum_{i=0}^7 \frac{(E_{data}^i - E_{prof}^i(\alpha, T, E))^2}{(\delta E_i(\alpha, T, E))^2}$$

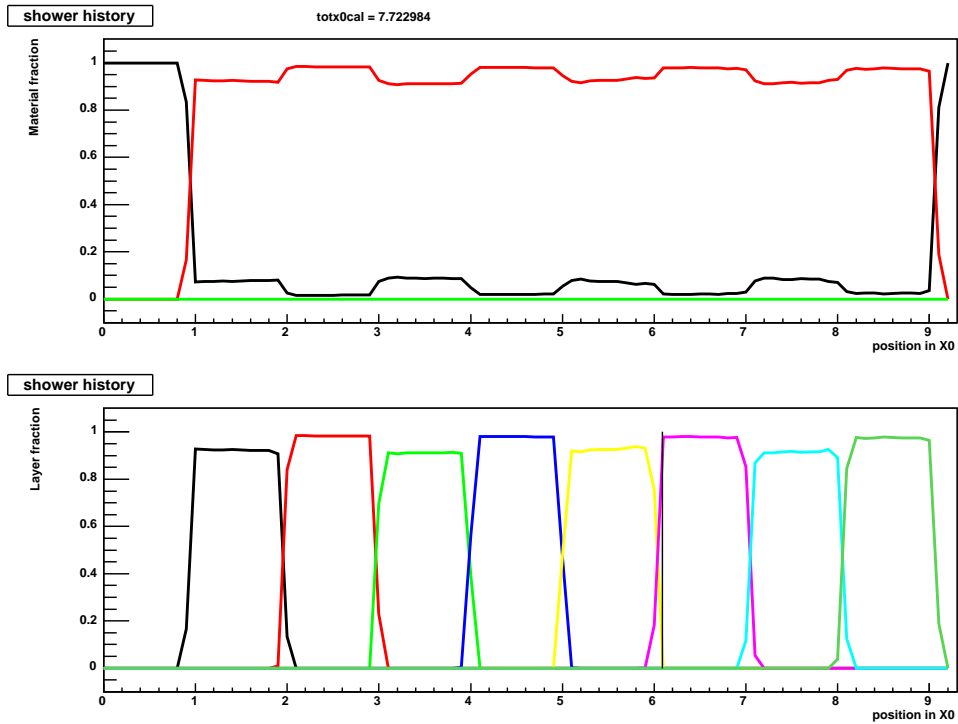


Figure 10: Shower development of one on-axis gamma far from cracks. Top : fraction of the shower in the “void” (black), inside CsI (red) and inside cracks (green). Bottom : fraction of the energy deposited in each layer.

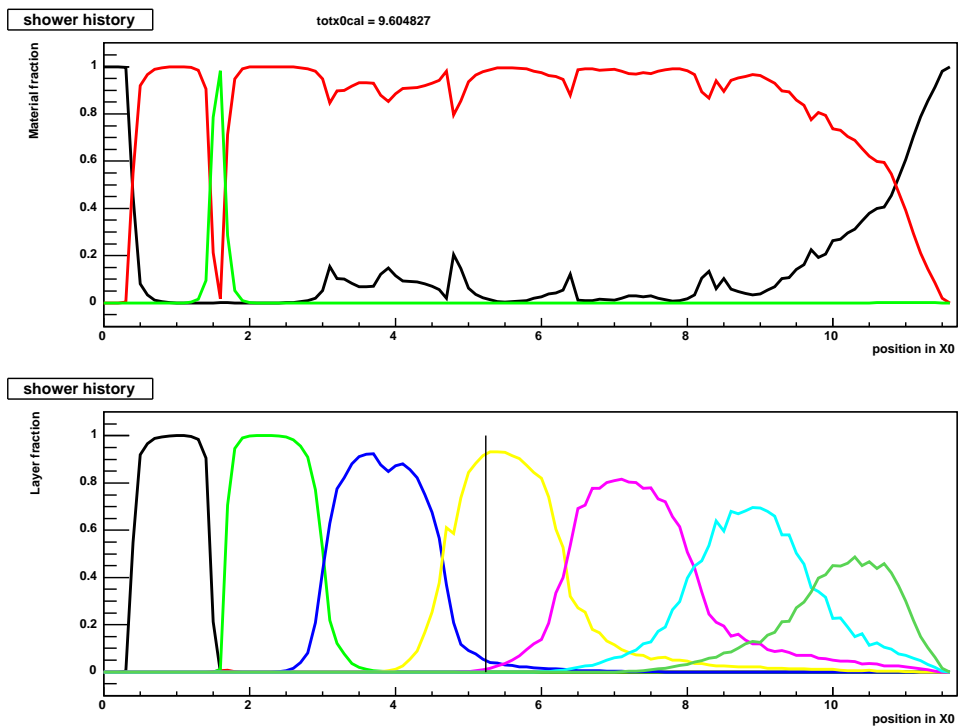


Figure 11: Same as figure 10 but for a gamma with an incoming angle = 50° . The vertical line shows the position of the maximum of the shower.

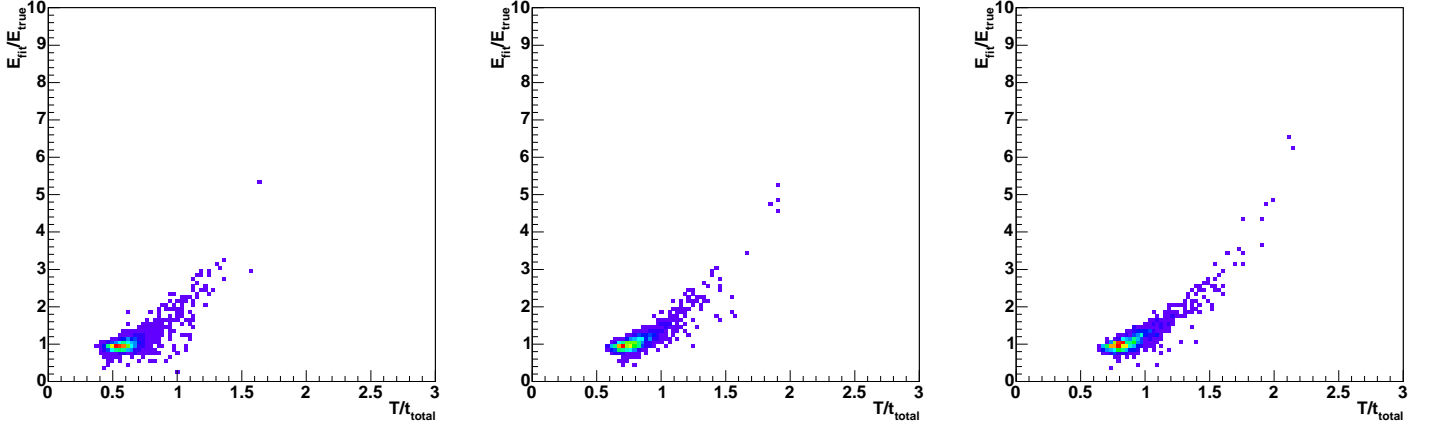


Figure 12: E_{fit}/E_{true} as function of T/t_{total} for 10 (left), 50 (center) and 100 GeV (right) on axis gammas in a LAT-like simulation when no constraint on the parameters is applied during the fit.

where (α, T, E) are the three free parameters of the fit, E_{data}^i the energies measured in the layers and $\delta E_i(\alpha, T, E)$ the modelization error. The dependence of χ_{std}^2 with T is not trivial because of the geometry dependence of $E_{prof}^i(\alpha, T, E)$ with T (due to the radial profile dependence with T).

The **Geant4** simulation presented in section 3.1 can be used to quickly simulate the on-axis LAT situation. This is done by considering the first $1.4 X_o$ as the tracker, and the following eight $1.1 X_o$ slices as the calorimeter layers. Only events for which the conversion point lies in the first $1.4 X_o$ are taken into account. Minimizing χ_{std}^2 generally allows a good determination of the energy but it fails when the shower is poorly contained. The ratio T/t_{tot} is used to estimate the shower containment. Figure 12 shows E_{fit}/E_{true} as function of T/t_{tot} for 10, 50 and 100 GeV gammas. It can be seen that when the shower maximum found by the fit lies outside the calorimeter ($T > t_{tot}$) the energy found by the fit largely overestimates the true energy. The higher the gamma energy is, the more often it happens.

In order to constrain the parameters (α, T) during the fit, the following term is added :

$$\chi_{par}^2(\alpha, T, E) = \frac{1}{1 - \rho^2(E)} \left(\frac{(\ln \alpha - \overline{\ln \alpha}(E))^2}{\sigma_{\ln \alpha}^2(E)} + \frac{(\ln T - \overline{\ln T}(E))^2}{\sigma_{\ln T}^2(E)} + 2\rho(E) \frac{(\ln \alpha - \overline{\ln \alpha}(E)) (\ln T - \overline{\ln T}(E))}{\sigma_{\ln \alpha}(E) \sigma_{\ln T}(E)} \right)$$

and the χ^2 minimized during the fit is now :

$$\chi_{tot}^2(\alpha, T, E) = \chi_{std}^2(\alpha, T, E) + c\chi_{par}^2(\alpha, T, E)$$

where c is the weight of the constraint.

The weight of the constraint should be chosen so as to avoid the high energy tail and to get the best resolution. In order to do so, the same **Geant4** simulation has been used to roughly simulate gammas in the LAT with a non zero incoming angle by simply considering the first $1.4/\cos\theta X_o$ as the tracker and the following eight $(1.1/\cos\theta) X_o$ slices as the calorimeter layers (the effect of cracks and the energy mixing between layers are not taken into account with this rough simulation). Figure 13 shows how the resolution varies with c and the incoming angle for 5, 10, 50 and 100 GeV gammas in such a LAT-like simulation. For on-axis gammas, not constraining α and T (i.e. $c = 0$) gives the worst resolution because of the importance of the high energy tail. The resolution first decreases with c and reaches a kind of plateau when $c \simeq 3$. When the incoming angle increases (i.e. the showers are more and more contained), the resolution exhibits a minimum (especially for 5 and 10 GeV gammas). The existence of such a minimum and the fact that the position of this minimum decreases with the incoming angle demonstrate that the more the showers are contained, the freer should the parameters α and T remain during the fit.

In the present implementation of **CalFullProfile** in **Gleam**, c has been set to 3 (because only the on-axis situation had been considered). Figure 14 shows the histogram of E_{fit}/E_{true} when no constraint is applied and when $c = 3$. It can be seen that the constraint on α and T avoids the high energy tail.

In order to further minimize the risk of overestimating the energy, one should increase the constraint

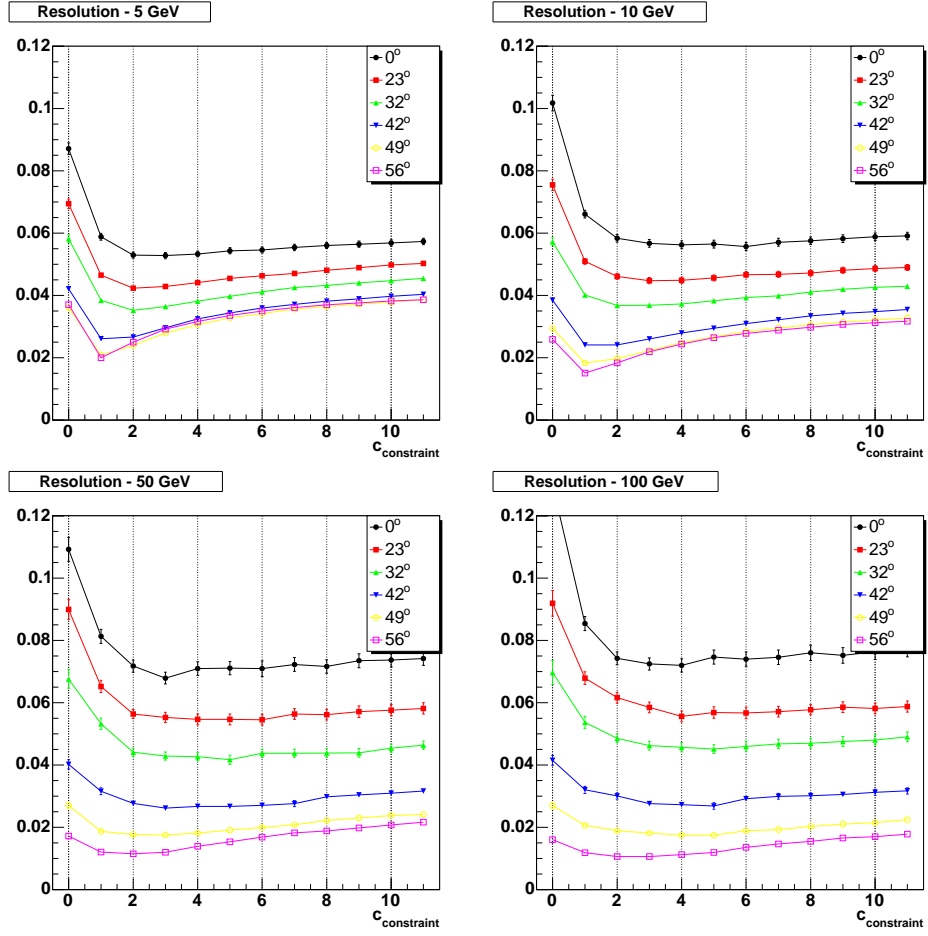


Figure 13: Resolution as function of the weight of the constraining term in χ^2_{tot} for various incoming angles for 5, 10, 50 and 100 GeV gammas in a LAT-like simulation.

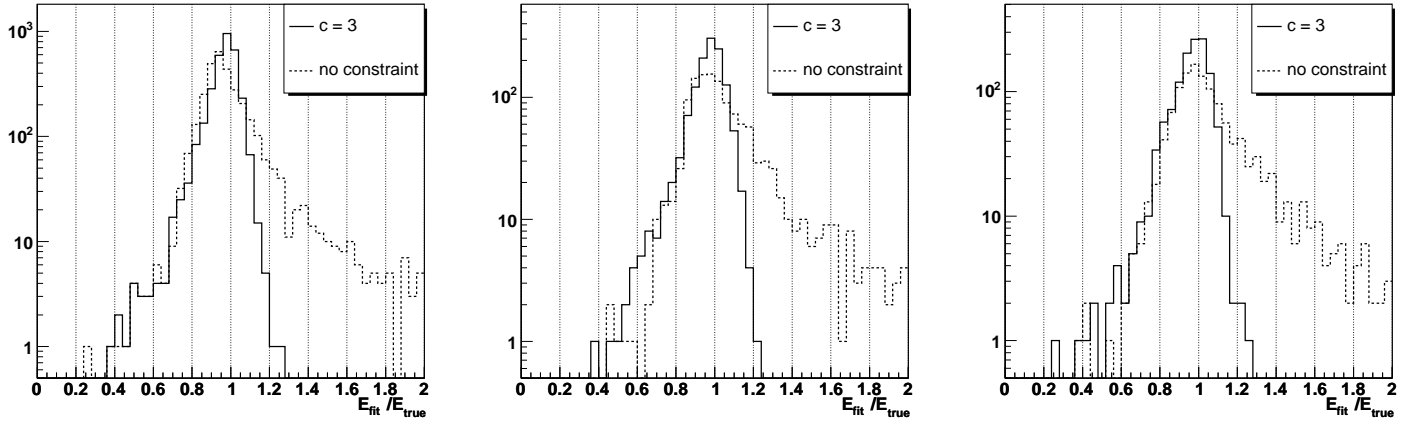


Figure 14: Histogram of $E_{\text{fit}}/E_{\text{true}}$ when no constraint is applied and when the weight of the constraining term in χ^2_{tot} is 3 for 10 (left), 50 (center) and 100 GeV (right) on axis gammas in a LAT-like simulation.

when the shower is poorly contained. This is done by defining c as the following function of T/t_{tot} :

$$c(T/t_{tot}) = \begin{cases} 3 & \text{if } T/t_{tot} < 0.9 \\ 3 + (T/t_{tot} - 0.9) & \text{otherwise} \end{cases}$$

6 Fit procedure for each event

For the sake of clarity, here is a short description of the whole fit procedure :

- reference trajectories in radiation units are computed for $T = 2, 3, 4, \dots, 14, 15, 16$;
- parameters initialization : the calorimeter raw energy E_{raw} is used as the starting value for E . The starting values for α and T are $e^{\overline{\ln \alpha}(E_{raw})}$ and $e^{\overline{\ln T}(E_{raw})}$;
- during each iteration with the set of parameters (α, T, E) :
 - compute the trajectory in radiation units corresponding to T by interpolating between the two adjacent reference trajectories;
 - compute the deposited energies in the layers $E_{prof}^i(\alpha, T, E)$;
 - compute the modelization error $\delta E_i(\alpha, T, E) = \epsilon(E) \times \max_{i \in [1,8]}(E_{prof}^i(\alpha, T, E))$
 - compute $\overline{\ln \alpha}(E)$, $\sigma_{\ln \alpha}(E)$, $\overline{\ln T}(E)$, $\sigma_{\ln T}(E)$ and $\rho(E)$;
 - compute $\chi_{tot}^2(\alpha, T, E)$.
- the following quantities are written in the merit tuple :
 - **CalCfpEnergy** : the energy given by the fit corrected for the bias due to the method ($\text{bias}(E)$);
 - **CalCfpEffRLn** : the effective radiation length in the CsI of the trajectory in radiation units corresponding to T_{fit} ;
 - **CalCfpChiSq** : the minimum of χ_{tot}^2 .

The algorithm runs when the raw energy in the calorimeter is larger than 1 GeV and when the total radiation length is greater than $0.5 X_0$.

7 First results and first improvements

This algorithm was first implemented in **CalRecon** in the beginning of July 2005. The first allgamma production running this energy correction tool was **allGamma-GR-HEAD1.594-merit-TKR-prune.root**. In order to check the results of **CalFullProfile**, the 3 following cuts are applied :

- **CalCfpEnergy**>0
- **acos(McXDir*VtxXDir+McYDir*VtxYDir+McZDir*VtxZDir)**<0.1
- **CalCfpEffRLn**>4

The first cut only requires that the algorithm has run. The second one ensures that the direction information used by the algorithm (i.e. the tracker information for tracker events) is good (the main effect of this cut is to strongly deplete the region $\text{McZDir}>-0.2$). The third one rejects events for which the amount of radiation length is not large enough to provide sufficient information. Figure 15 shows how the resolution and the relative bias vary with **CalCfpEffRLn**. When **CalCfpEffRLn**<4 the bias is large and the resolution is poor.

Figure 16 shows the reconstructed energy divided by the true energy as function of the logarithm of the true energy and the cosine of the incoming angle. This first glance to the results is rather satisfactory except for the fact that for large incoming angles the energy tends to be underestimated (it can be seen in figure 21(left) that the negative bias can be as large as -8%).

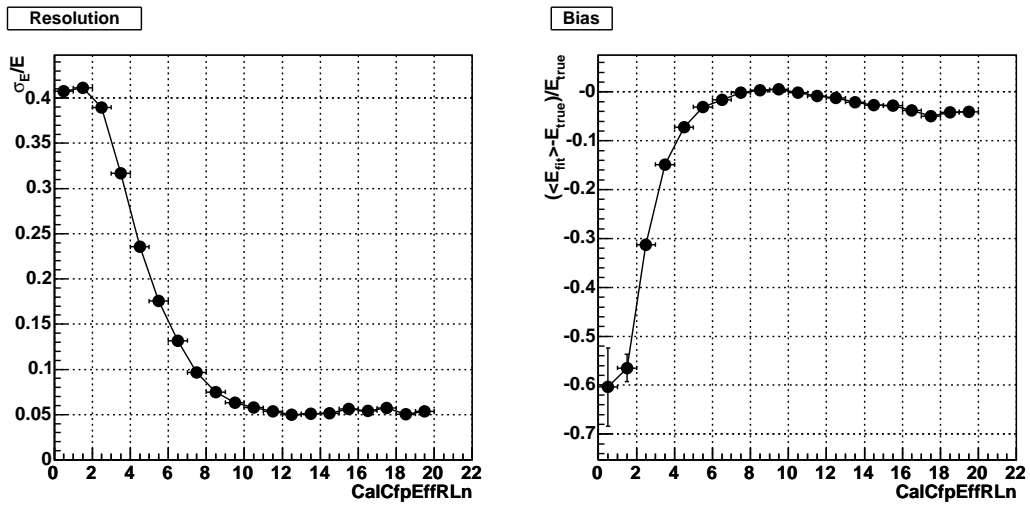


Figure 15: Resolution and relative bias as function of the effective radiation length in the CsI. (GR-HEAD1.594)

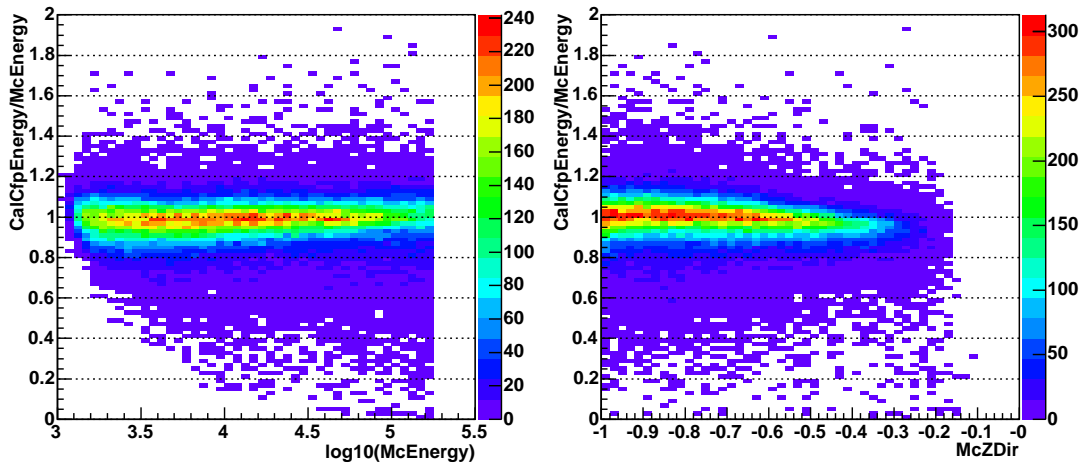


Figure 16: The reconstructed energy divided by the true energy as function of the logarithm of the true energy for all angles (left) and the cosine of the incoming angle for all energies (right). (GR-HEAD1.594)

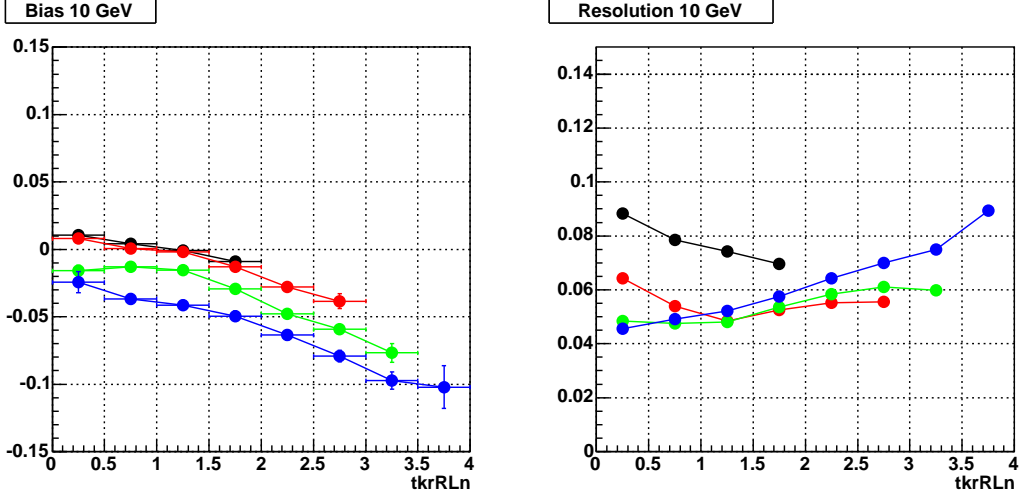


Figure 17: Relative bias and resolution as function of the radiation length in the tracker for 10 GeV gammas with an incoming angle of 0° (black), 50° (red), 60° (green), 70° (blue).

Since the negative bias at large incoming angle is seen only for tracker events and not for cal-only events, it is likely related to the amount of radiation length in the tracker t_{tkr} , which obviously increases when the incoming angle increases. Figure 17 shows the bias and the resolution as function of t_{tkr} for 10 GeV gammas with an incoming angle of 0, 50, 60 and 70° . At fixed incoming angle, the bias exhibits a clear dependence with t_{tkr} . At fixed t_{tkr} , there is a lighter variation with the incoming angle.

The translation of the trajectory in radiation length units presented in section 4 does not compute the development of the shower in the tracker. It only uses the amount of radiation length in the tracker (computed by considering the shower as a straight line) as an input. The radial extension of the shower is taken into account only while studying the trajectory within the calorimeter. The radial profile in the tracker is expected to be larger than in the calorimeter since the distance between the converter layers in the tracker is large whereas the distance between the CsI layers in the calorimeter is negligible. This effect is expected to be rather small when t_{tkr} is small (i.e. close to on-axis) but figure 17 shows that it should be certainly corrected for when $t_{tkr} > 2$.

In order to correct for this effect, it is chosen to widen artificially the radial profile of showers rather than studying the development of the shower in the tracker as accurately as in the calorimeter. Figure 18 shows how the bias changes when the radial profile is widened. It is clear from this figure that the widening factor should depend on t_{tkr} . The increase of the bias with the incoming angle seen in figure 17 implies that the widening factor should also depend on the incoming angle.

The analysis of how the bias varies with t_{tkr} for various incoming angles leads to the following empiric function of the widening factor $f_{wid}(\theta, t_{tkr})$:

$$f_{wid}(\theta, t_{tkr}) = \begin{cases} 1 & \text{if } \theta < 40 \\ 1 & \text{if } \theta > 40 \text{ and } t_{tkr} < t_{tkr}^{min}(\theta) \\ \min(2, 1 + (t_{tkr} - t_{tkr}^{min})/1.5) & \text{if } \theta > 40 \text{ and } t_{tkr} > t_{tkr}^{min}(\theta) \end{cases}$$

where θ is in degrees and $t_{tkr}^{min} = 2 - 0.05(\theta - 40)$.

Figure 19 shows the same as figure 17 but when the radial profile is increased by the factor $f_{wid}(\theta, t_{tkr})$. It can be seen that the dependences of the bias with the incoming angle and the radiation length in the tracker are considerably reduced.

Figure 20 shows the same as figure 16 after the radial profile widening correction was implemented. Figure 21 shows that after this correction the energy is no more systematically underestimated at large incoming angles.

There is no widening correction for $\theta < 40^\circ$ as can be seen in the definition of $f_{wid}(\theta, t_{tkr})$. Figure 22 shows the effect of widening the radial profile of on axis 10 GeV gammas. It can be seen that the best resolution is really given by not widening the radial profile, providing further confidence in the radial profile used by

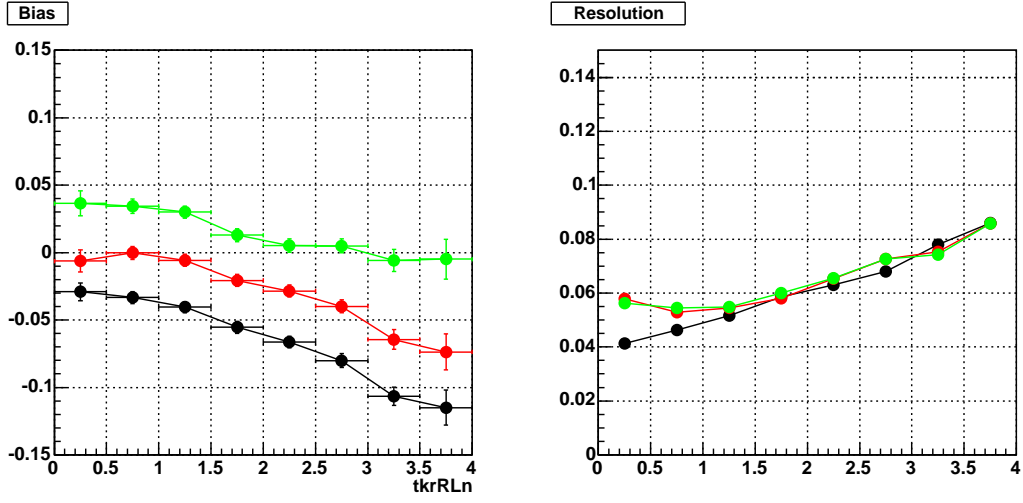


Figure 18: Relative bias and resolution as function of the radiation length in the tracker for 10 GeV gammas with an incoming angle of 70° for different values of the widening factor : 1 (black), 1.5 (red) and 2 (green).

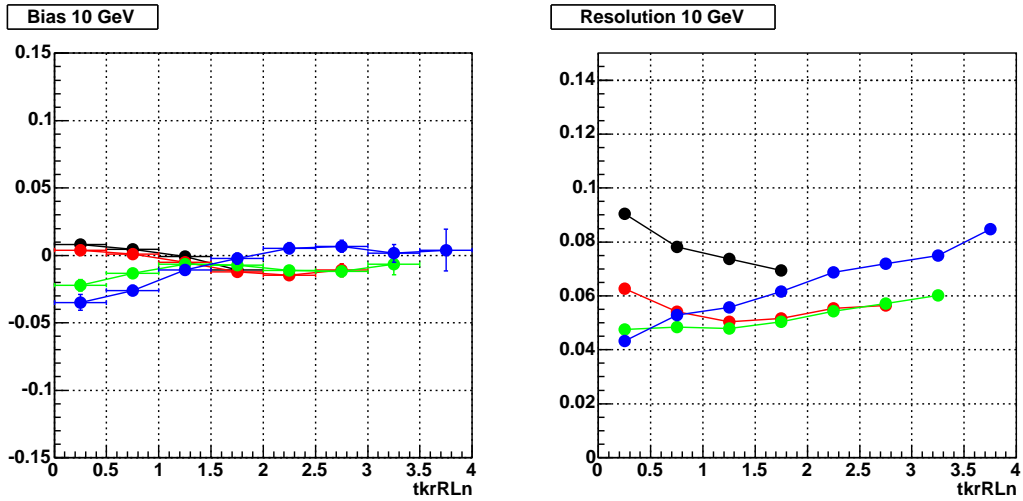


Figure 19: Relative bias and resolution as function of the radiation length in the tracker for 10 GeV gammas with an incoming angle of 0° (black), 50° (red), 60° (green), 70° (blue) when the radial profile is increased by the factor $f_{wid}(\theta, t_{tkr})$.

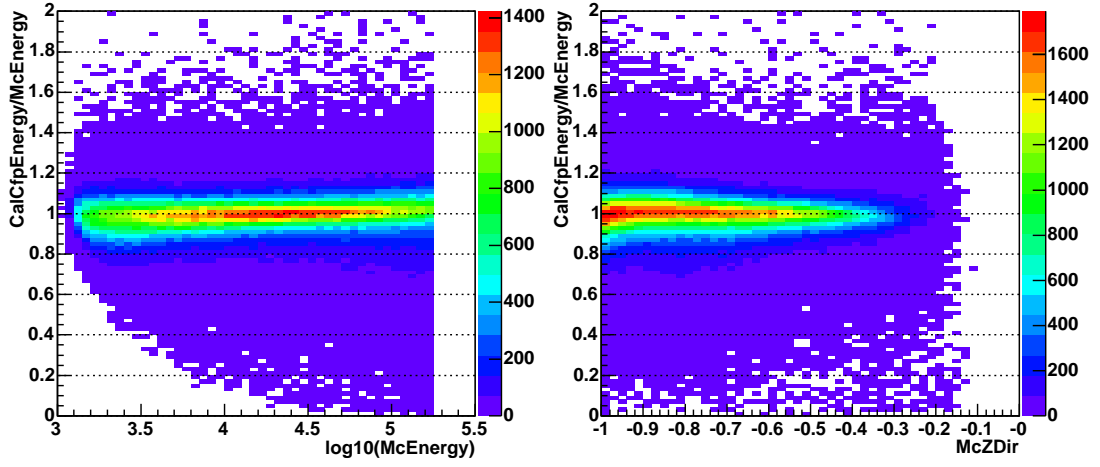


Figure 20: The reconstructed energy divided by the true energy as function of the logarithm of the true energy (left) and the cosine of the incoming angle (right). (GR-HEAD1.635)

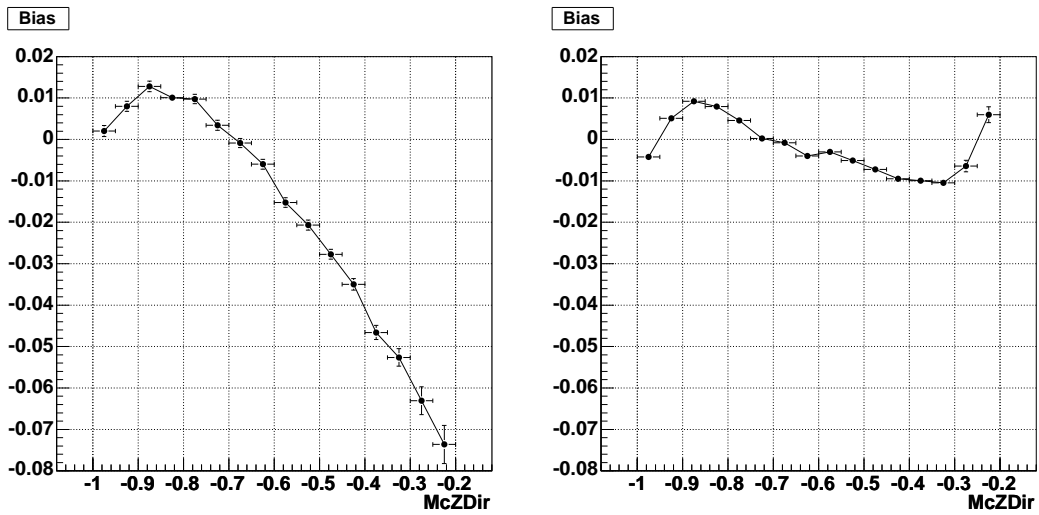


Figure 21: The relative energy bias as function of the cosine of the incoming angle for all energies before (left : GR-HEAD1.594) and after (right : GR-HEAD1.635) the radial profile widening correction was implemented.

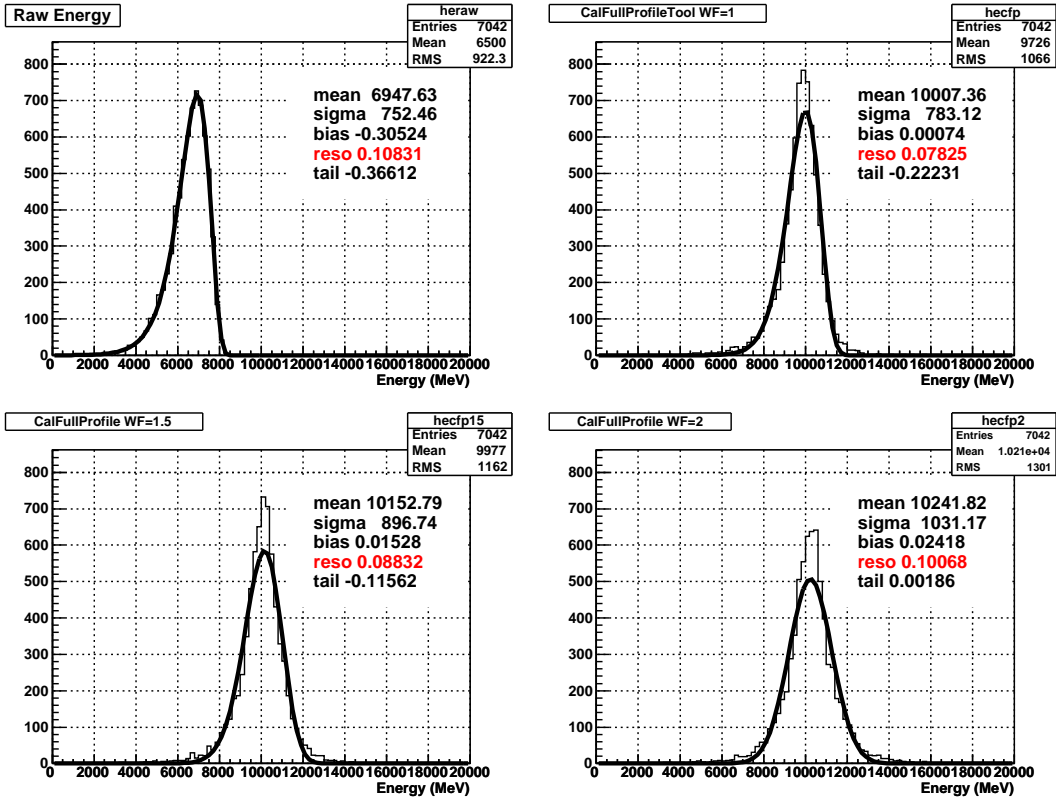


Figure 22: For on axis 10 GeV gammas, histogram of $\text{CalEnergyRaw}/\text{McEnergy}$ (top left) and $\text{CalCfpEnergy}/\text{McEnergy}$ for different values of the widening factor : 1 (top right), 1.5 (bottom left) and 2 (bottom right).

CalFullProfile . It means that the effective radius of the showers at the beginning of their development is rather small : 68% of the energy is contained in a radius of $R_M/10$ when $t/T \lesssim 0.5$. It is interesting to note that the distance between two adjacent CsI logs (the width of the carbon cell structure) is 1.14 mm, which is not completely negligible compared to $R_M/10 = 3.5$ mm. CalFullProfile takes into account the distance between CsI logs while computing the development of the showers into the calorimeter and this is the reason why the curves in figure 10 have a crenel shape (the gamma passes between two CsI Y logs and in the middle of one X log).

8 Performances near cracks

One of the motivations to use the radial profile is the case of gammas passing near cracks. The effect of cracks is maximal for on-axis gammas. Figure 23 shows the fraction of energy deposited in the calorimeter and the effective amount of radiation lengths in the calorimeter versus the maximum of the X and Y distances to the center of the closest tower for 10 GeV on-axis gammas. The deposited energy decreases as the gammas get closer to the crack. The decrease near the logs boundaries is due to the carbon cell array. The effective amount of radiation length in the CsI exhibits the same behaviour.

Figure 23(top) shows the ratio of the reconstructed energy over the true energy as function of the maximum of the X and Y distances to the center of the closest tower. This ratio is 1 in average even very close to the boundary of the last log, which proves that taking into account the radial profile allows a good estimation of the effective amount of radiation length in the CsI and a good reconstruction of the energy. It is also interesting to note that the arch shape due to the cell carbon array has disappeared. Figure 23(bottom) shows that requiring that CalCfpEffRLn is large enough can remove gammas for which the energy resolution is not good.

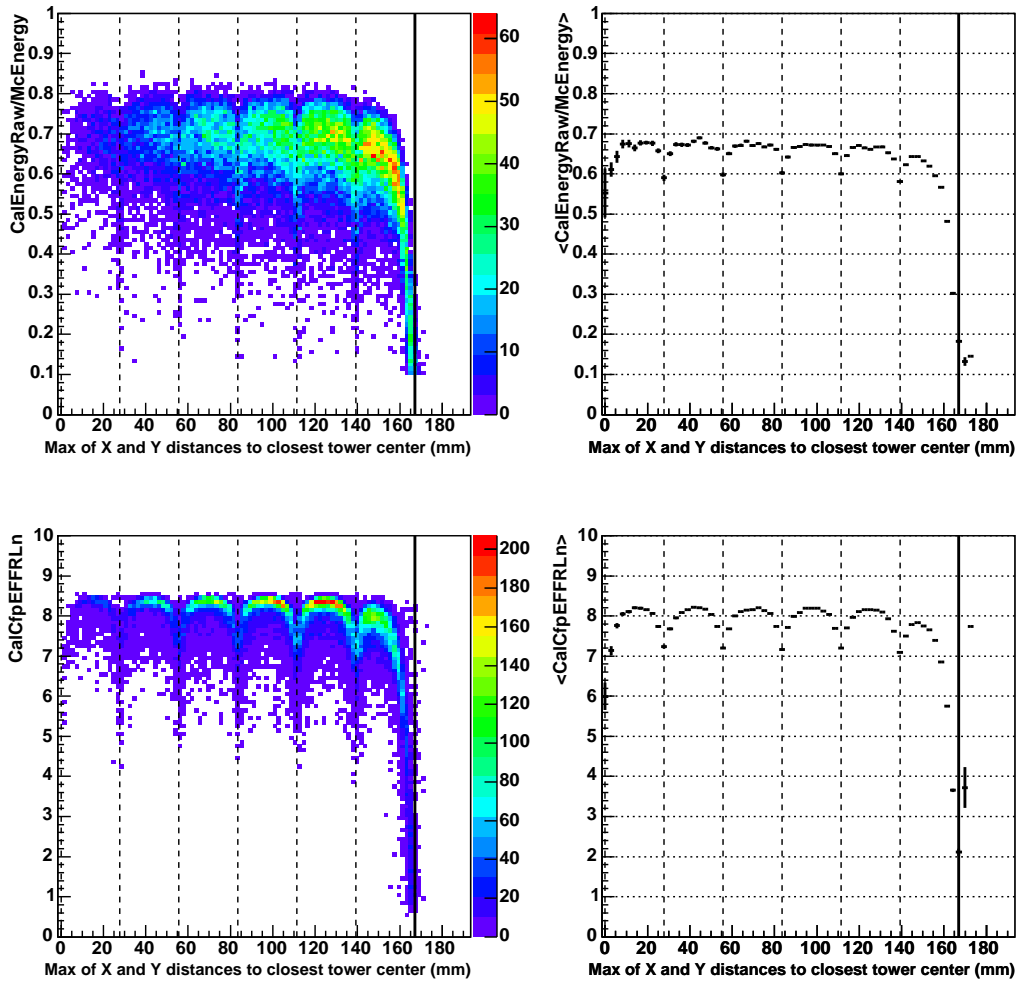


Figure 23: The fraction of energy deposited in the calorimeter (top), the effective amount of radiation lengths in the CsI (bottom) versus the maximum of the X and Y distances to the center of the closest tower for 10 GeV on-axis gammas, when CalFullProfile has run. The vertical dashed lines show the logs boundaries. The vertical solid line shows the boundary of the last log. (GR-v7r2)

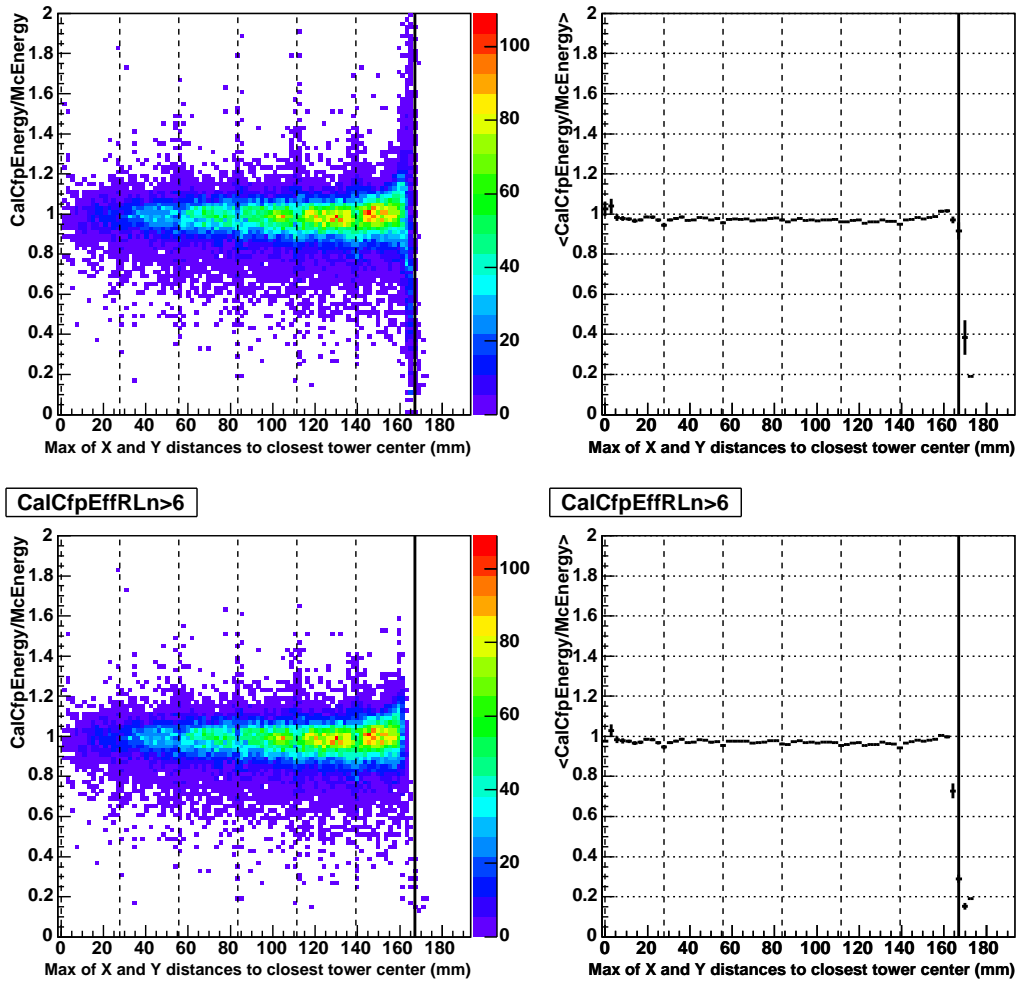


Figure 24: The ratio of the reconstructed energy over the true energy versus the maximum of the X and Y distances to the center of the closest tower for 10 GeV on-axis gammas before (top) and after (bottom) requiring $\text{CalCfpEffRLn} > 6$. The vertical dashed lines show the logs boundaries. The vertical solid line shows the boundary of the last log. (GR-v7r2)

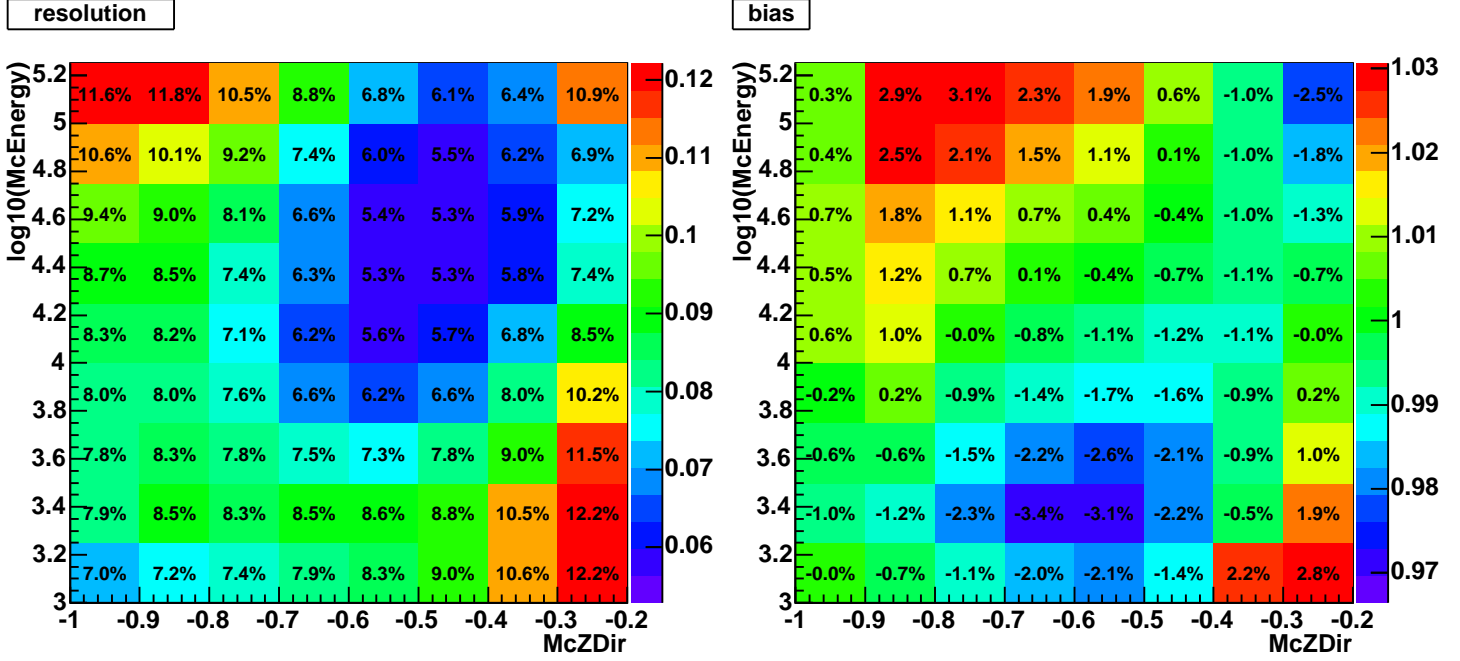


Figure 25: Resolution and relative bias as function of the cosine of the true incoming angle and the logarithm of the true energy for tracker events. (GR-HEAD1.635)

9 Performances for tracker events

Figure 25 shows the resolution and the bias as function of the cosine of the true incoming angle and the logarithm of the true energy for tracker events. As in the previous section, the following cuts are applied :

- $\text{CalcFpEnergy} > 0$
- $\text{acos}(\text{McXDir} \cdot \text{VtxXDir} + \text{McYDir} \cdot \text{VtxYDir} + \text{McZDir} \cdot \text{VtxZDir}) < 0.1$
- $\text{CalcFpEffRLn} > 4$

The bias is small over the whole phase space. The resolution behaves as expected :

- when on axis, the resolution degrades when the energy increases because the showers are less and less contained;
- at fixed energies, the resolution improves when the incoming angle increases because the showers are in average more contained;
- but this is no longer true at low energy or at very large incoming angles because the fraction of the energy deposited in the tracker can be large and because the gammas can go out of the calorimeter through its sides.

For these reasons the resolution histogram exhibits a clear minimum region corresponding to $50 \lesssim \theta \lesssim 70^\circ$ and $10 \lesssim E \lesssim 100 \text{ GeV}$.

10 Performances for cal-only events

Figure 26 shows the resolution and the bias as function of the cosine of the true incoming angle and the logarithm of the true energy for cal-only events. The following cuts are applied :

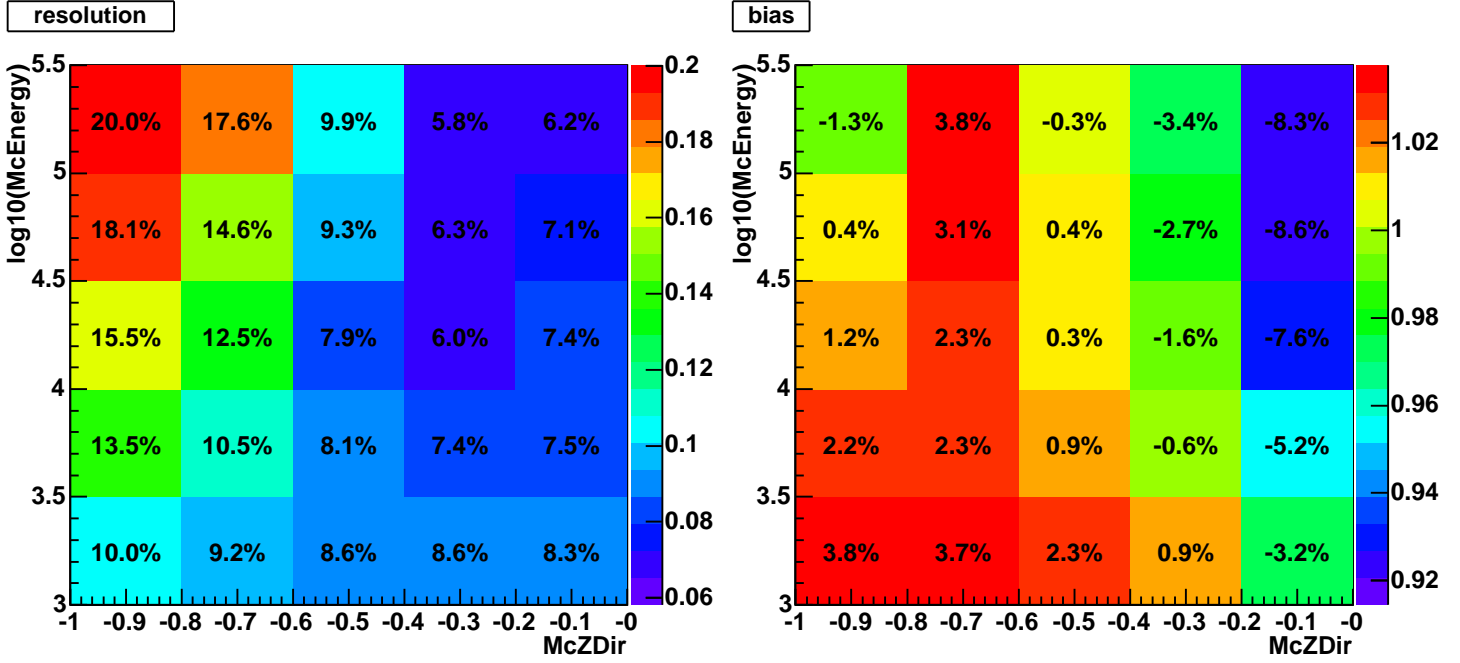


Figure 26: Resolution and relative bias as function of the cosine of the true incoming angle and the logarithm of the true energy for cal-only events. (GR-v7r0p2)

- $\text{CalCfpEnergy} > 0$
- $\text{acos}(\text{McXDir} * \text{CalXDir} + \text{McYDir} * \text{CalYDir} + \text{McZDir} * \text{CalZDir}) < 0.2$
- $\text{CalCfpEffRLn} > 4$

Compared to the case of tracker events, the resolution is generally worse for cal-only events since the showers are less contained in average, except at large incoming angles where no more energy is deposited in the tracker. The bias is rather small except for very large incoming angles.

11 Conclusion

The performances of `CalFullProfile` are rather satisfactory, especially for gammas passing through cracks (the energy loss is well estimated) and for very high energy gammas (no high energy tail). Some improvements are still needed :

- further optimizing the choice of the weight of the constraining term;
- using the calorimeter direction information when the tracker information is not good;
- using the tower segmentation at very large incoming angles;
- estimating the event energy error.

Optimizing the weight of the constraint should help to improve the resolution of rather well contained low energy gammas (less than ~ 10 GeV) as can be seen in figure 13. But this figure was made with a LAT-like simulation. So it has to be checked that these results are still valid for the real LAT situation, i.e. with cracks and energy mixing between layers.

At very large incoming angles, the tracker direction information is not very accurate because of backplash effects. This is why the current energy given by `CalFullProfile` is not good when the incoming angle is very large ($\text{McZDir} > -0.2$). It is possible to use the distance between the centroid of the calorimeter cluster to the tracker trajectory to choose either the calorimeter or the tracker direction informations [4].

When the incoming angle is very large, the shower axis is almost parallel to the layer planes. As a consequence, the layer structure does not provide information about the longitudinal shape of showers anymore. In this configuration, the tower segmentation should be used on top of the layer segmentation.

Estimating the event energy error is very interesting because it would help to compare the several existing energy reconstruction algorithms (last layer, parametric) when using classification trees, and because it can be used for low statistics analysis. But it is not obvious since the error given by the fit cannot be used directly. This is because of the constraining term $c\chi_{par}^2$ in χ_{tot}^2 .

Acknowledgements

I would like to thank my GLAST colleagues at LLR, Pol d’Avezac and Berrie Giebels, for their help during my first steps in the GLAST analysis and many fruitful discussions. I would like to thank Marc Verderi for his help in using `Geant4` and Denis Bernard for the very fruitful discussion on how constraining the parameters during the fit. I would like to stress that the implementation of `CalFullProfile` in `GLEAM` was really easy due to the re-write of `CalRecon` and especially the part concerning the energy correction tools.

References

- [1] R. Terrier, see :
www-glast.slac.stanford.edu/software/Workshops/September00Workshop/RegisEnergyRecon.pdf
- [2] E. Longo and I. Sestili, *Nucl. Instrum. Methods* **128**, 283 (1975)
- [3] G. Grindhammer and S. Peters, “The parameterized simulation of electromagnetic showers in homogeneous and sampling calorimeters”, presented at the International Conference on Monte Carlo Simulation in High-Energy and Nuclear Physics - MC 93, Tallahassee, Florida, 22-26 Feb 1993 (hep-ex/0001020).
- [4] Ph. Bruel, “Trajectory and energy reconstruction”, see :
www-glast.slac.stanford.edu/software/AnaGroup/Philippe_analysis_20050815.pdf.